ARTICLE

Supporting Information

Interfacial C–S Bonding Stabilizes Phase-Tailored Ni Heterosulfides on Carbon Nanofibers for Bifunctional Electrolytic Water Splitting

Abdul Qadir [a], Kejian Wang [b,], Agasthiyaraj Lakshmanan [c], Raza Ullah [d], Mohamedazeem M. Mohideen [a], Alamgir [c], Abdurohman Mengesha Yessuf [a], Yong Liu [a,*]*

a. Beijing Key Laboratory of Advanced Functional Polymer Composites, College of Materials Science and Engineering, Beijing University of Chemical Technology, Beijing 100029, China
b. College of Mechanical and Electrical Engineering, Beijing University of Chemical Technology, Beijing 100029, China
c. School of Materials Science and Engineering, Zhejiang Sci-Tech University, Hangzhou, Zhejiang 310018, China
d. School of Materials Science and Engineering, Shandong University of Technology, Zibo, Shandong 255000, China

DFT Studies:

DFT calculation was studied using the CASTEP module in Materials Studio 2020. Generalized Gradient Approximation (GGA) and Perdew–Burke–Ernzerhof (PBE) were used to find out the band structure and density of states (DOS) of the developed structure. TS was used for DFT-D correction. Also, 380 eV was kept for the kinetic energy cutoff with a 2 x 2 x 3 k-point grid for geometry optimization and energy calculations. In order to prevent the formation of bulk aggregates, the cubic arrangement has also been downscaled to nanostructured domains, thereby facilitating effective interfacial coupling on the CNF support. This has resulted in enhanced active site exposure, as well as improved catalytic performance. Norm-conversing pseudopotential was used to understand the interactions between the electron and the ion core. All simulations were studied at 2 x 10-5 energy convergence with 0.05 and 0.002 maximum atomic forces and displacement.

HER and OER reaction co-ordinates were evaluated based on the following steps.

HER pathway

Mechanism for HER is represented by the following equation.

$H^+ + e^- \longrightarrow H^*$

$NiS_x\text{-CNF} + H^* \rightarrow NiS_x\text{-CNF} + 1/2H_2$

OER Path way:

Mechanism for OER is shown by the following figure

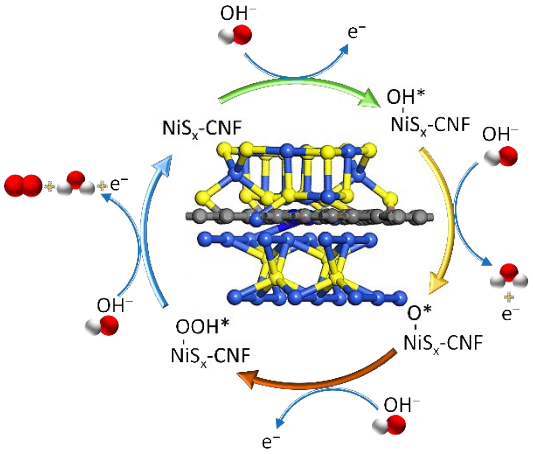

Fig. S1: Schematic representation of the OER mechanism.

For computational Gibbs free energy HER reactions, the computational hydrogen electrode (CHE) model was applied. The electron-hole pair transfer was included using the equations of ΔGn (U) = ΔGn(0) + neU, where n is (H^+ + e). Therefore, a chemical potential of 0.5 H_2 was applied to equate the (H^+ + e) combination at 0 V of RHE at standard conditions. The Gibbs free energy was calculated using ΔG = EDFT +ZPE – TS, where EDFT, ZPE, TS, and Esolv are DFT-calculated, zero-point, and entropic energy values, respectively.

Determination of Tafel slopes and electrochemical active surface area (ECSA):

The Tafel slope was calculated via the subsequent equation:
η = a + blog(j)

In this expression, η signifies the overpotential, a is the intercept associated with the exchange current density (j_0), b represents the Tafel slope, and j defines the current density.

Electrochemical active surface area (ECSA):

The ECSA was evaluated by calculating the double-layer capacitance (C_{dl}) from cyclic voltammetry (CV) curves recorded within the non-Faradaic region at different scan rates. For HER and OER studies, the non-Faradaic potential range selected was from 0.1 to 0.2 V and 1.08 to 1.18. The C_{dl} was determined using the following equation:

$$C_{dl} = \frac{|janodic - jcathodic|}{2v}$$

where j_{anode} and $j_{cathode}$ denote the anodic and cathodic current densities, respectively, and v represents the scan rate. The ECSA was then calculated using the equation:

$$ECSA = \frac{Cdl}{C\square\_s}$$

Here, C_s is the real capacitance of a standard surface, typically ranging from 20 to 60 μF/cm² in 1 M KOH solutions for most transition metal compound-based materials. In this study, a standard value of 40 μF/cm² was employed for C_s.

Determination of Turnover Frequency:

The TOF (s^{-1}) is determined using the subsequent equation:

$$TOF = \frac{I}{mNF}$$

In this context, "I" signifies the current at a specified applied potential, "N" indicates the number of moles of active sites on the electrode surface (mol), "F" represents the Faraday constant (C mol^{-1}), and "M" defines the number of transferred electrons (where M = 2 for the HER and M = 4 for the OER).

$$N = \frac{Q}{2F} = \frac{I*t}{2F} = \frac{I*V/u}{2F} = \frac{Q}{2F*u}$$

Where Q denotes the integrated effective area in cyclic voltammetry (CV), F signifies Faraday's constant, and μ indicates the scan rate (20 mV s^{-1}).

Determination of Mass Activity

Mass activity quantitatively assesses catalytic performance, defined as the current produced per gram of catalyst at a specified overpotential. The calculation was performed utilising the relationship:

$$\text{Mass activity} = \frac{I}{m}$$

where I represent the current (A) at a designated voltage and m denotes the mass of catalyst deposited on the electrode.

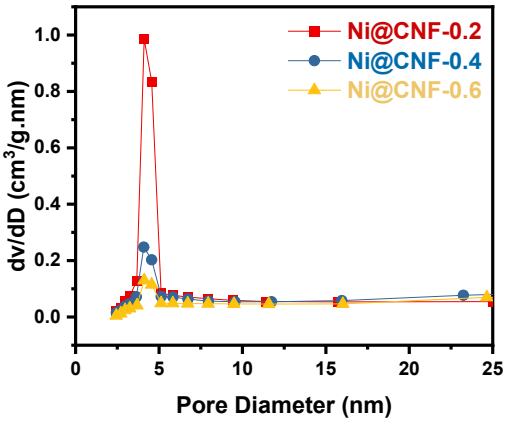

Fig. S2: Pore size distributions of Ni@CNF composites.

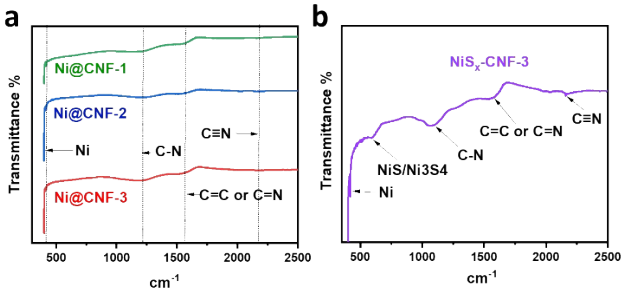

Fig. S3: FTIR spectra of (a) Ni@CNF composites with varying Ni concentrations, showing characteristic peaks for Ni, C–N, and C≡N groups. (b) NiS_x–CNF-3, highlighting the presence of NiS/Ni_3S_4, Ni, C–N, and C≡N functional groups.

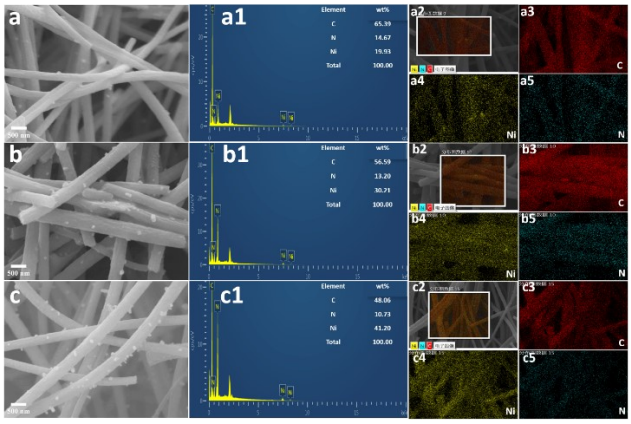

Fig. S4: SEM images, EDS spectra, and elemental mapping of Ni@CNF composites: (a) Ni@CNF-0.2, (b) Ni@CNF-0.4, and (c) Ni@CNF-0.6; (a1), (b1), and (c1) represent the corresponding EDS spectra; (a2), (b2), and (c2) show elemental mapping of C, N, and Ni, confirming uniform distribution within the nanofiber structure.

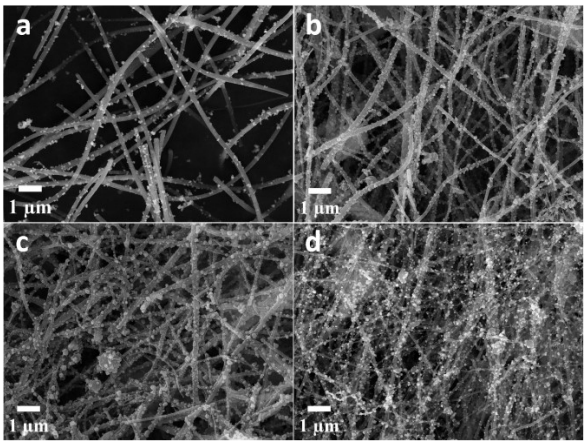

Fig. S5: SEM images of NiS_x-CNF composites: (a) NiS_x-CNF-1, (b) NiS_x-CNF-2, (c) NiS_x-CNF-3, and (d) NiS_x-CNF-4, showing the nanofiber morphology and distribution of nickel sulfide particles.

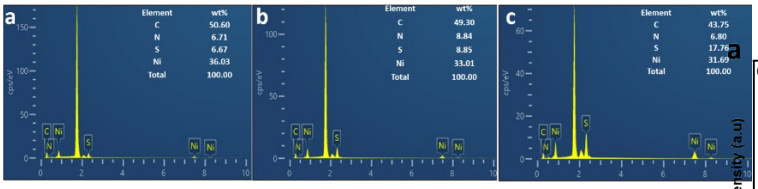

Fig. S6: EDS spectra of (a) NiS_x-CNF-1, (b) NiS_x-CNF-2, and (c) NiS_x-CNF-4, showing the elemental composition of C, N, S, and Ni.

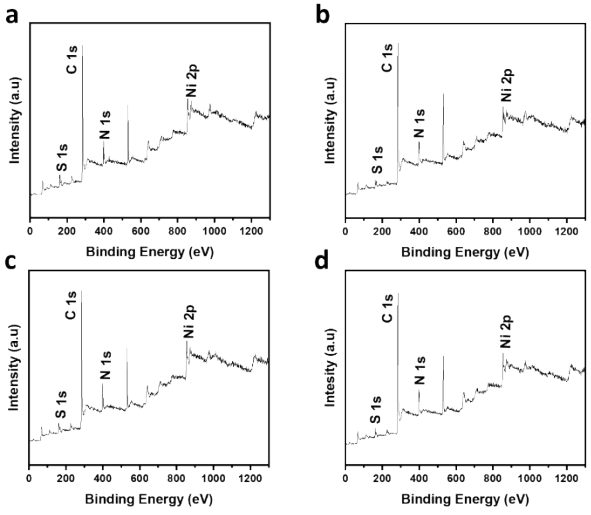

Fig. S7: XPS survey spectra of NiS_x-CNF composites: (a) NiS_x-CNF-1, (b) NiS_x-CNF-2, (c) NiS_x-CNF-3, and (d) NiS_x-CNF-4.

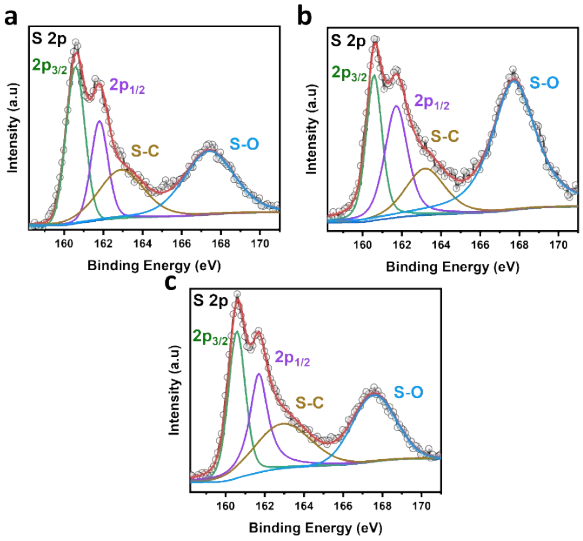

Fig. S8: Deconvoluted XPS S 2p spectra of NiS_x-CNF composites: (a) NiS_x-CNF-1, (b) NiS_x-CNF-2, (c) NiS_x-CNF-4.

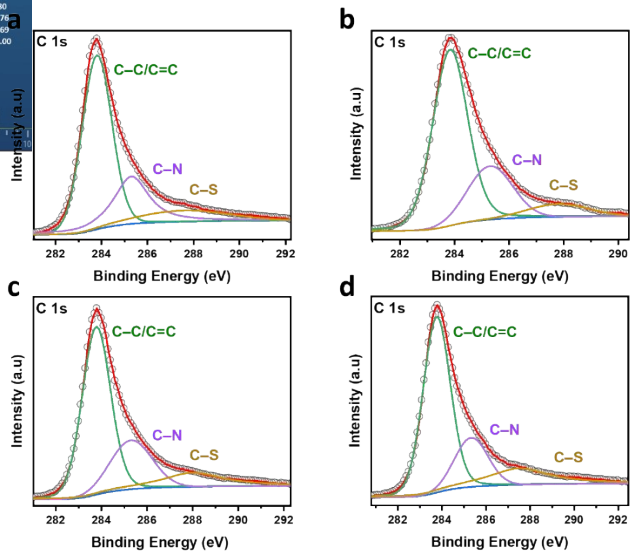

Fig. S9: Deconvoluted XPS C 1s spectra of NiS_x-CNF composites: (a) NiS_x-CNF-1, (b) NiS_x-CNF-2, (c) NiS_x-CNF-3, and (d) NiS_x-CNF-4.

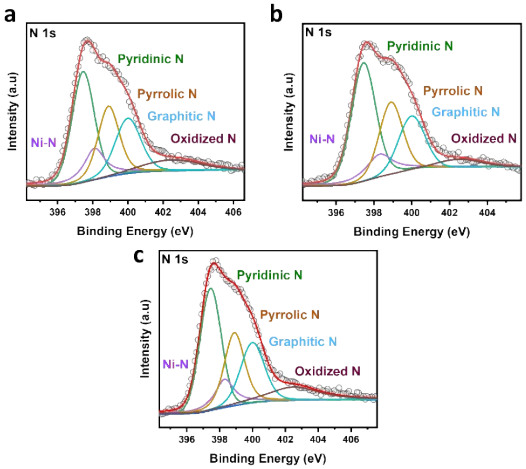

Fig. S10: Deconvoluted XPS N 1s spectra of NiS_x-CNF composites: (a) NiS_x-CNF-1, (b) NiS_x-CNF-2, (c) NiS_x-CNF-4

Table S1: Phase Fractions of Ni, NiS and Ni_3S_4 in various NiS_x-CNF Composites.

NiS_x-CNF-1			NiS_x-CNF-2			NiS_x-CNF-3			NiS_x-CNF-4		
Ni^0	NiS	Ni_3S_4	Ni^0	NiS	Ni_3S_4	Ni^0	NiS	Ni_3S_4	Ni^0	NiS	Ni_3S_4
26.90%	57.46%	15.63%	20.03%	49.01%	30.96%	20.55%	34.54%	44.90%	0%	13.58%	86.42%

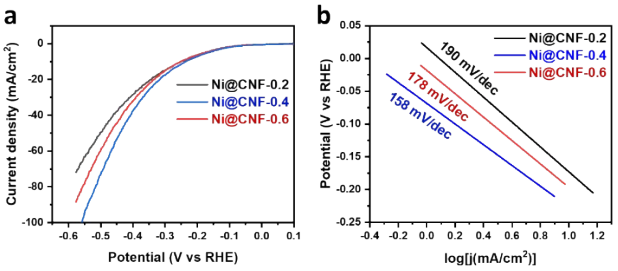

Fig. S11: Electrocatalytic performance of Ni@CNF composites: (a) Polarization curves and (b) corresponding Tafel plots for Ni@CNF-0.2, Ni@CNF-0.4, and Ni@CNF-0.6.

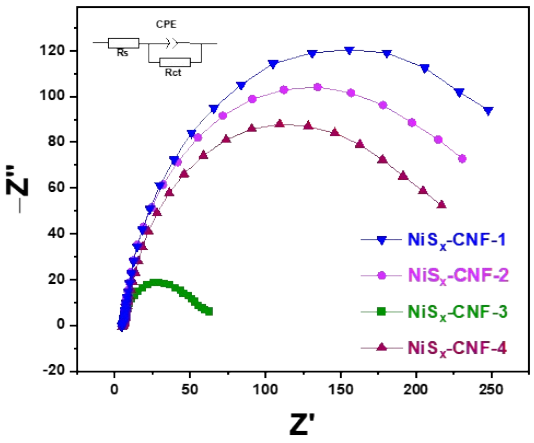

Fig. S12: (a) OER EIS (Electrochemical Impedance Spectroscopy) Nyquist plots of the catalysts.

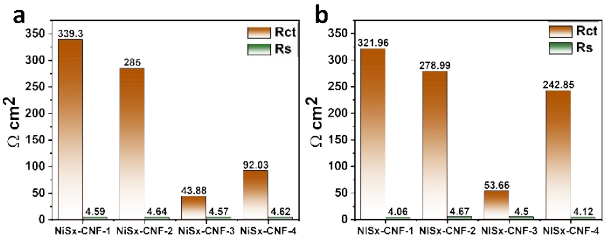

Fig. S13 EIS fitting data plots for (a) HER and (b) OER, showing charge transfer resistance (R_{ct}) and solution resistance (R_s).

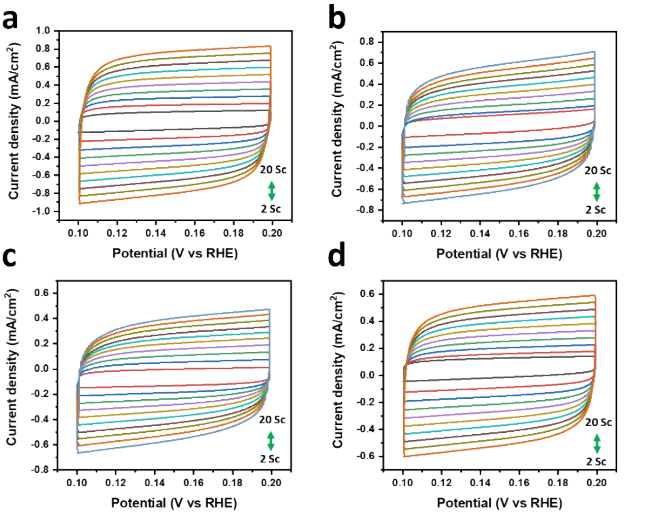

Fig. S14: Cyclic voltammetry for HER curves at different scan rates for (a) NiS_x-CNF-3, (b) NiS_x-CNF-4, (c) NiS_x-CNF-1, and (d) NiS_x-CNF-2.

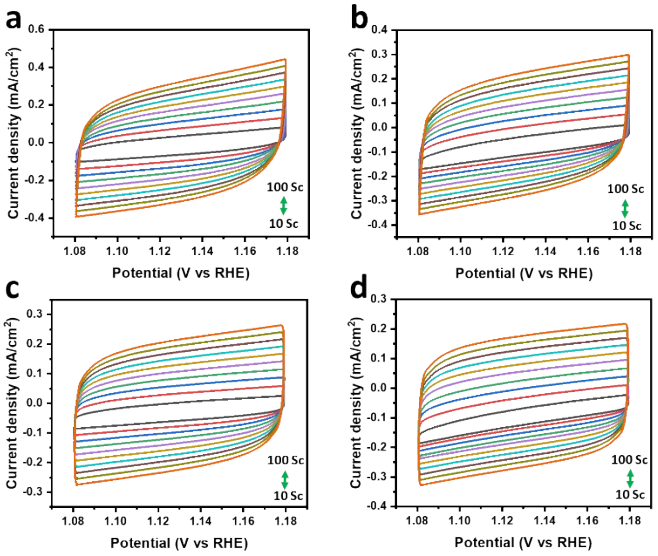

Fig. S15: Cyclic voltammetry curves for OER at different scan rates for (a) NiS_x-CNF-1, (b) NiS_x-CNF-2, (c) NiS_x-CNF-3, and (d) NiS_x-CNF-4.

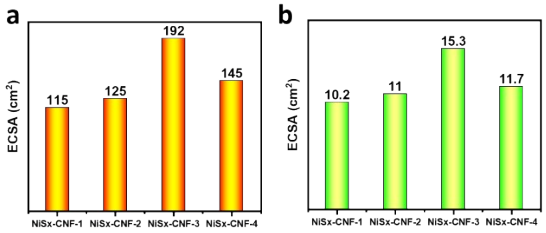

Fig. S16: ECSA values for NiS_x–CNF composites in (a) HER and (b) OER.

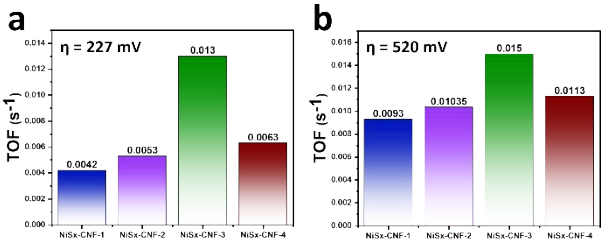

Fig. S17. TOF values of (a) HER and (b) OER for all the prepared catalysts at an overpotential of η = 227 mV and η = 520 mV.

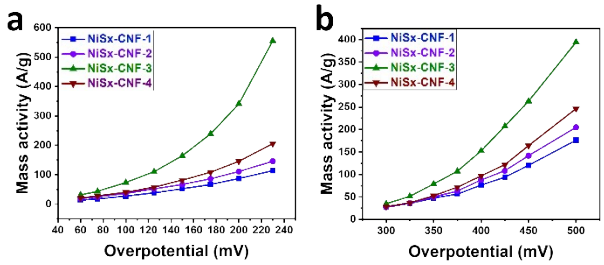

Fig. S18. Mass activity curves of (a) HER and (b) OER for NiSx-CNF-1, NiSx-CNF-2, NiSx-CNF-3, and NiSx-CNF-4 catalysts at various overpotentials

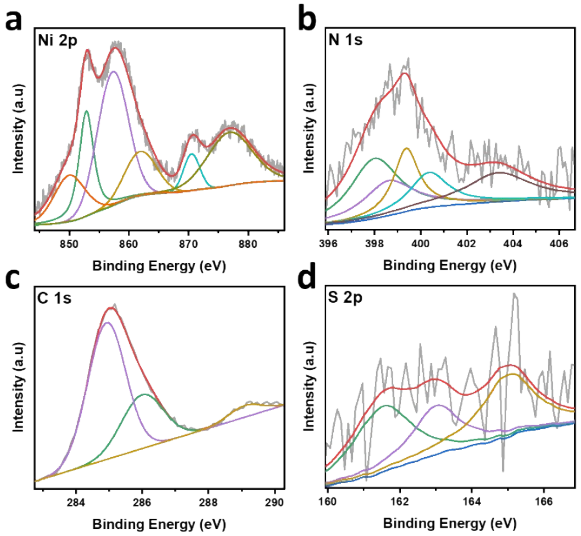

Fig. S19: Post-HER activity XPS analysis of NiS_x-CNF composites showing the deconvolution peaks for Ni 2p, Ni 1s, C 1s, and S 2p regions.

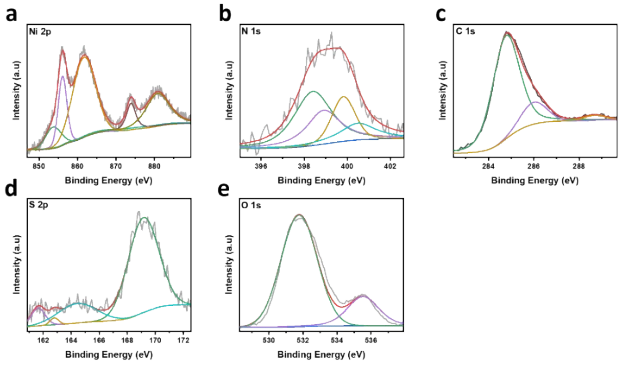

Fig. S20: Post-OER activity XPS analysis of NiS_x-CNF composites showing the deconvolution peaks for Ni 2p, Ni 1s, C 1s, S 2p, and O 1s regions.

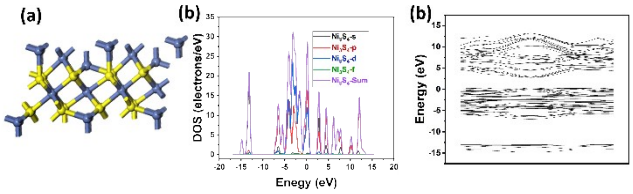

Fig. S21 (a) Optimized structure, (b) Band structure, and (c) DOS of Ni_3S_4.

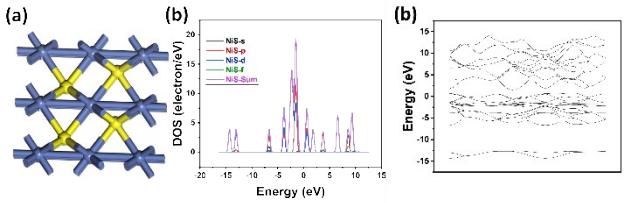

Fig. S22 (a) Optimized structure, (b) Band structure, and (c) DOS of NiS.

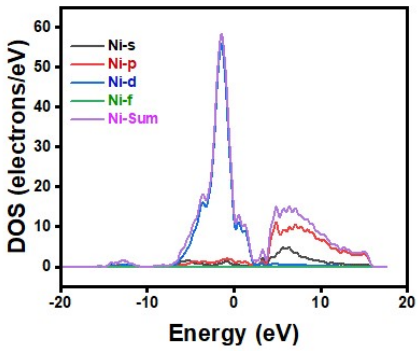

Fig. S23 represent DOS of Ni.

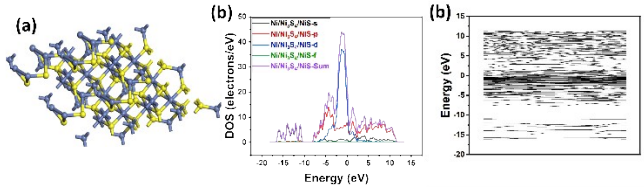

Fig. S24 (a) Optimized structure, (b) Band structure, and (c) DOS of Ni/Ni3S4/NiS.

Table S2: Comparison of HER performance of NiS_x-CNF-3 with previously reported catalysts.

Electrode	Electrolyte	η (mV@mA/cm^2)	TS_{HER} (mV/dec)	Ref.
NiS_x-CNF-3	1.0 M KOH	88@10	34	This work
Cu_2S-Ni_3S_2	1.0 M KOH	149@10	75.89	1
Cox/Ni_3S_2@NFCOS	1.0 M KOH	204@10	113.13	2
Mn-NiS	1.0 M KOH	99@10	64.8	3
CoMoP/Ni_3S_2	1.0 M KOH	97@10	63	4
NiAl-LDH/Ni_3S_2/NF	1.0 M KOH	209@10	68.7	5
V_s-Ru-Ni_9S_8	1.0 M KOH	94@10	69.8	6
NF@G-5@Ni_3S_2	1.0 M KOH	119@10	64.8	7
α-NiS@NDCDs/NF	1.0 M KOH	173@10	81	8
NCDs/Ni_3S_2/NF	1.0 M KOH	149@10	72	9
Ni/NiS/P,N,S-Rgo	1.0 M KOH	155@10	135	10
Ni/Ni_3C/C-NCNT	1.0 M KOH	184@10	98.7	11
N-doped NiMoS	1.0 M KOH	68@10	86	12
NiS/Ni_3S_4/GCW	1.0 M KOH	91@10	89	13
$Fe_{11.1\%}$-Ni_3S_2/NF	1.0 M KOH	89@10	89	14
Ni3S2@MoS_2/FeOOH	1.0 M KOH	95@10	85	15
$FeMoS_2$/Ni_3S_2/NF-2	1.0 M KOH	131@10	113	16
Ni_3S_2-S	1.0 M KOH	240@10	96	17
CoP/NCNHP	1.0 M KOH	115@10	66	18
Co-NC/CF	1.0 M KOH	157@10	109	19

Table S3: Comparison of OER performance of NiS_x-CNF-3 with previously reported catalysts.

Electrode	Electrolyte	η (mV@mA/cm^2)	TS_{HER} (mV/dec)	Stability (h)	Ref.
NiS_x-CNF-3	1.0 M KOH	330@10	45	55	This work

NiS/NF	1.0 M KOH	335@50	89	20	[20]
W_2N/WC	1.0 M KOH	320@10	122	-	[21]
$Cu_{50}Ni_{50}$	1.0 M KOH	318@10	63	20	[22]
NiS/NiS_2	1.0 M KOH	358@10	-	36	[23]
W-$CoS_{1.097}$/$CoSe_2$	1.0 M KOH	400@10	21.3	24	[24]
Ag_2O/NiO	1.0 M KOH	430@10	98	30	[25]
NiFeII-PBA	1.0 M KOH	285@10	53.1	12	[26]
Ni–Co_3O_4	1.0 M KOH	310@10	59	10	[27]
$NiCoO_4$	1.0 M KOH	350@10	43	-	[28]
Spinel $NiCo_2O_4$ nanoflowers on graphene	1.0 M KOH	383@10	137	1	[29]

Table S4: Comparison of Overall water splitting performance of NiS_x-CNF-3 with previously reported catalysts.

Catalyst	Cell Voltage (V) at 10 mA/cm^2	Journal name	Publication Year	Ref.
Ru-Ni_3S_2/NF	1.67 V	*Materials Science & Technology*	2025	[30]
MoS_2-$NixS_6$/NF	1.67	*International Journal of Hydrogen Energy*	2025	[31]
NMS	1.69	*ACS Applied Energy Materials*	2025	[32]
Fe/W-Ni_3S_2	1.69	*Small*	2024	[33]
$CuCo_2S_4$/$NiCo_2S_4$	1.66	*International Journal of Hydrogen Energy*	2024	[34]
S-NiFe-LDH	1.67	*Journal of Alloys and Compounds*	2024	[35]
S_v-Co_3S_4/MoS_2	1.67	*Inorganic Chemistry*	2023	[36]
P–CoMoOTe$_2$	1.68	*International Journal of Hydrogen Energy*	2025	[37]
Ni_3S_2@MnO_2@NF	1.68	*ChemSusChem*	2026	[38]
MoS_2/$NiFe_2O_4$	1.69	*International Journal of Hydrogen Energy*	2024	[39]
Co@CNR	1.66	*ACS APPLIED NANO MATERIALS*	2025	[40]
$Fe_{0.95}S_{1.05}$	1.68	*International Journal of Energy Research*	2023	[41]
NiS_x-CNF-3	1.65			**This work**

References:

1. K. S. Bhat and H. J. Nagaraja, *ChemistrySelect*, **2020,** *5*, 2455.
2. S. Shit, S. Chhetri, W. Jang, N. C. Murmu, H. Koo, P. Samanta, T. Kuila and J. Kuila, *ACS Appl. Mater. Interfaces*, **2018,** *10*, 27712.
3. Z. Hou, D. Xiang, D. Yang, L. Wen, H. Luo, L. Li, Q. Yang and L. Hu, *J. Therm. Energy Syst.*, **2022,** *169*, 106512.
4. M. B. Poudel, N. Logeshwaran, A. R. Kim, S. Karthikeyan, S. Vijayapradeep and D. J. Yoo, *J. Alloys Compd.*, **2023,** *960*, 170678.
5. L. Zhao, Z. Guo and Z. Liu, *J. Alloys Compd.*, **2022,** *910*, 164880.
6. Q. Gao, W. Luo, X. Ma, Z. Ma, S. Li, F. Gou, W. Shen, Y. Jiang, R. He and M. Li, *Appl. Catal. B: Environ.*, **2022,** *310*, 121356.
7. C. Jin, N. Zhou, Y. Wang, X. Li, M. Chen, Y. Dong, Z. Yu, Y. Liang, D. Qu and Y. Dong, *J. Electroanal. Chem.*, **2020,** *858*, 113795.
8. C. Pitchai, S. M. Gopalakrishnan and C.-M. Chen, *Energy Fuels*, **2024,** *38*, 2235.
9. Y. Rao, H. Ning, X. Ma, Y. Liu, Y. Wang, H. Liu, J. Liu, Q. Zhao and M. Wu, *Carbon*, **2018,** *129*, 335.
10. M. B. Z. Hegazy, M. R. Berber, Y. Yamauchi, A. Pakdel, R. Cao and U.-P. Apfel, *ACS Appl. Mater. Interfaces*, **2021,** *13*, 34043.
11. T. Dong, X. Zhang, Y. Cao, H.-S. Chen, P. Yang and F. Yang, *Inorg. Chem. Front.*, **2019,** *6*, 1073.
12. C. Huang, L. Yu, W. Zhang, Q. Xiao, J. Zhou, Y. Zhang, P. An, J. Zhang and Y. Yu, *Appl. Catal. B: Environ.*, **2020,** *276*, 119137.
13. Z. Jiang, L. Zheng, C. Sheng, H. Xu, S. Chen, Y. Liao, Y. Qing and Y. Wu, *J. Colloid Interface Sci.*, **2022,** *626*, 848.
14. W. Zhu, Z. Yue, W. Zhang, N. Hu, Z. Luo, M. Ren, Z. Xu, Z. Wei, Y. Suo and J. Wang, *J. Mater. Chem. A*, **2018,** *6*, 4346.
15. M. Zheng, K. Guo, W.-J. Jiang, T. Tang, X. Wang, P. Zhou,

J. Du, Y. Zhao, C. Xu and J.-S. Hu, *Appl. Catal. B: Environ.*, **2019,** *244*, 1004.
16. J.-Y. Xue, F.-L. Li, Z.-Y. Zhao, C. Li, C.-Y. Ni, H.-W. Gu, P. Braunstein, X.-Q. Huang and J.-P. Lang, *Dalton Trans.*, **2019,** *48*, 12186.
17. S. Zubaid, J. Khan and T. A. Sherazi, *J. Colloid Interface Sci.*, 2024, *660*, 502.
18. Y. Pan, K. Sun, S. Liu, X. Cao, K. Wu, W.-C. Cheong, Z. Chen, Y. Wang, Y. Li and Y. Liu, *J. Am. Chem. Soc.*, **2018,** *140*, 2610.
19. H. Huang, S. Zhou, C. Yu, H. Huang, J. Zhao, L. Dai and J. Qiu, *Energy Environ. Sci.*, **2020,** *13*, 545.
20. W. Zhu, X. Yue, W. Zhang, S. Yu, Y. Zhang and J. Wang, *Chem. Commun.*, **2016,** *52*, 1486.
21. J. Diao, Y. Qiu, S. Liu, W. Wang, K. Chen, H. Li, W. Yuan, Y. Qu and X. Guo, *Adv. Funct. Mater.*, **2020,** *32*, 1905679.
22. E. Gioria, S. Li, A. Mazheika, R. Naumann d'Alnoncourt, A. Thomas and F. Rosowski, *Angew. Chem. Int. Ed.*, **2023,** *135*, e202217888.
23. Q. Li, D. Wang, C. Han, X. Ma, Q. Lu, Z. Xing and X. Yang, *J. Mater. Chem. A*, **2018,** *6*, 8233.
24. X. Yang, G. Sui, D. Guo, D. Chu, J. Li, S. Na, M. Yu and D. Li, *Inorg. Chem.*, **2023,** *29*, 4115.
25. Z. Shaghaghi and S. Akbari, *Int. J. Hydrogen Energy*, **2024,** *51*, 936.
26. Y. Zeng, G.-F. Chen, Z. Jiang, L.-X. Ding, S. Wang and H. Wang, *J. Mater. Chem. A*, **2018,** *6*, 15942.
27. L. Zeng, K. Zhou, L. Yang, G. Du, L. Liu and W. Zhou, *Adv. Energy Mater.*, **2018,** *1*, 6279.
28. C. Broicher, F. Zeng, J. Artz, H. Hartmann, A. Besmehn, S. Palkovits and R. Palkovits, *ChemCatChem*, **2019,** *11*, 412.
29. Z. Li, B. Li, J. Chen, Q. Pang and P. Shen, *Int. J. Hydrogen Energy*, **2019,** *44*, 16120.
30. Li, R.; Guo, B.; Bian, Z.; Chang, J.; Zhang, J.; Wang, J.; Zhang, H.; Li, W.; Feng, X. *J. Mater. Sci. Technol.* **2025**, *238*, 313.
31. Mao, Y.; Geng, L.; Zhang, Q.; Zhang, L.; Zeng, Y.; Sim, L. B. *Int. J. Hydrogen Energy* **2025**, *137*, 95.
32. Sharan, H.; Kausalya, A.; Lakshmipathi, S.; Madhavan, J.; Karthikesan, P.; Mani, A. *ACS Appl. Energy Mater.* **2025**, *8*, 13752.
33. Wang, S.; Yuan, D.; Sun, S.; Huang, S.; Wu, Y.; Zhang, L.; Dou, S. X.; Liu, H. K.; Dou, Y.; Xu, J. *Small* **2024**, *20*, 2311770.
34. Joshi, K. K.; Chauhan, S. V.; Pataniya, P. M.; Sumesh, C. K. *Int. J. Hydrogen Energy* **2024**, *58*, 1562.
35. Zhang, S.; Ji, Y.; Wang, S.; Zhang, P.; Shi, D.; Lu, F.; Zhang, B. *J. Alloys Compd.* **2024**, *1002*, 175323.
36. He, Q.; Ye, N.; Han, L.; Tao, K. *Inorg. Chem.* **2023**, *62*, 21240.
37. Jian, Y.-J. J.; Perumal, S.; Sakthivel, M.; Lin, L.-Y.; Ho, K.-C. *Int. J. Hydrogen Energy* **2025**, *122*, 206.
38. Madan, C.; Singh, A.; Kumari, S.; Rana, K. S.; Soni, A.; Bera, C.; Halder, A. *ChemSusChem* **2026**, *19*, e202501816.
39. Ren, T.; Huang, X.; Chen, J.; Wang, G.; Liu, Y.; Bao, F.; Guo, W. *Int. J. Hydrogen Energy* **2024,** 57, 983.
40. Qadir, A.; Wang, K.; Mohideen, M. M.; Lakshmanan, A.; Ullah, R.; Alamgir,; Yessuf, A. M.; Huang, Y.; Shang, W.; Liu, Y. *ACS Appl. Nano Mater*. **2025**, 8, 23115.
41. Li, X.; Li, F.; Li, Q.; Li, H.; Ji, Z. *Int. J. Energy Res.* **2023**, 9275185.